AAPS PharmSciTech, Vol. 13, No. 4, December 2012 (© 2012)
DOI: 10.1208/s12249-012-9862-8

Research Article

The Improvement of the Anticancer Effect of a Novel Compound Benzoic Acid, 2-Hydroxy-, 2-D-ribofuranosylhydrazide (BHR) Loaded in Solid Lipid Nanoparticles

Mei Wang,[1] Lili Qin,[2,3] Kun Li,[3] Rongrong Zhu,[3] Wenrui Wang,[3] and Shilong Wang[3,4]

Received 23 June 2012; accepted 14 September 2012; published online 28 September 2012

Abstract. A novel drug delivery system consisting of benzoic acid, 2-hydroxy-, 2-D-ribofuranosylhydrazide (BHR)-loaded solid lipid nanoparticles (BHR-SLNs) was prepared using the emulsification–evaporation technique. The mean particle size of the BHR-SLNs measured by photon correlation spectroscopy was about 75 nm. BHR-SLN morphology was assessed by transmission electron microscopy and atomic force microscopy. The drug entrapment efficiency was 70.2%, as determined via Sephadex gel chromatography and high-performance liquid chromatography. Drug release assessment *in vitro* showed that BHR was gradually released from SLNs in a time-dependent manner. Furthermore, treatment of 293T and Hela cells with BHR-SLNs demonstrated that BHR-SLNs were less toxic to normal cells while more effective in antitumor potency compared with the BHR drug alone. The results imply that BHR-SLNs could be considered as a promising antitumor drug system for a range of new therapeutic applications.

KEY WORDS: benzoic acid, 2-hydroxy-, 2-D-ribofuranosylhydrazide (BHR); controlled release; drug delivery; solid lipid nanoparticles.

INTRODUCTION

Salicylic acid derivatives have been widely used to treat a variety of diseases. Recently, researches have become increasingly focused on their anticancer properties (1,2). For instance, salicylhydroxamic acid and salicylic acid derivatives have been shown to be involved in the inhibition of tumor cell proliferation (3,4). In a previous study, we synthesized a novel *N*-glycoside salicylic acid derivative, benzoic acid, 2-hydroxy-, 2-D-ribofuranosylhydrazide (BHR; Fig. 1), in an effort to find new anticancer drugs. We also characterized the photophysical and photochemical behaviors of BHR by means of laser flash photolysis and discussed the potential mechanism behind its anticancer effect (5). Cell-based assays *in vitro* not only demonstrated the inhibitory effect of BHR on the proliferation of Hela cells, but also revealed some toxicity of the compound to normal cells.

In recent years, nanomaterials have been more frequently employed as vehicles for controlled drug delivery (6–13). For instance, solid lipid nanoparticles (SLNs) have been introduced as an attractive alternative to traditional drug delivery systems (14–17). SLN use for topical application has been receiving more attention because of the numerous advantages it provides over conventional formulations (18,19). For example, it can protect labile compounds against chemical degradation (20), enhance the availability of drugs by promoting sustained release (21), and improve the efficiency of drugs by facilitating targeted delivery (22,23). Furthermore, the low toxicity of SLNs has allowed their frequent use as drug carriers (24,25). Thus, encapsulation of BHR in SLNs may enhance the anticancer effect of BHR while lowering its toxicity.

Therefore, a new drug delivery system composed of BHR loaded into SLNs (BHR-SLN) was synthesized in our present study. The physicochemical properties of BHR-SLNs, including particle size, stability, morphology, entrapment efficiency (EE%), and *in vitro* drug release behavior, were characterized. *In vitro* cellular assays indicated that SLNs improved the anticancer effect of BHR while reducing the toxicity of BHR to normal cells.

MATERIALS AND METHODS

Materials

BHR was generously supplied by Dr. Sichang Shao (Fuyang Normal College, Fuyang City, China) at a purity ≥99%, which was confirmed by high-performance liquid chromatography (HPLC). Stearic acid, lecithin, acetone, chloroform, Myrj 59, dimethyl sulfoxide (DMSO), and 3-(4,5-dimethylthiazol-2-yl)-2,5-diphenyltetrazolium bromide (MTT) were obtained from Sigma Chemical Co. (St. Louis, Missouri, USA). RPMI-1640, fetal calf serum (FCS), penicillin G, streptomycin, trypsinase, and phosphate-buffered saline (PBS, pH 7.4) were purchased from GIBCO BRL (Grand

Mei Wang and Lili Qin contributed equally to this work.

[1] Department of Chemistry, Tongji University, Siping Road 1239, Shanghai 200092, People's Republic of China.
[2] Department of Physical Education, Tongji University, Siping Road 1239, Shanghai 200092, People's Republic of China.
[3] School of Life Science and Technology, Tongji University, Siping Road 1239, Shanghai 200092, People's Republic of China.
[4] To whom correspondence should be addressed. (e-mail: wsl@tongji.edu.cn)

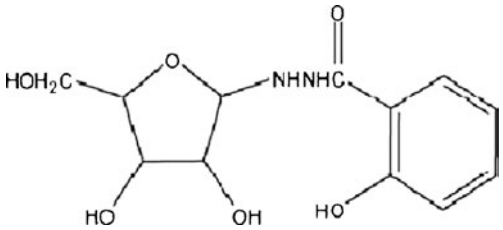

Fig. 1. Chemical structure of the *N*-glycoside salicylic acid derivative BHR

Island, New York, USA). All chemicals were of HPLC or analytical grade. The water used in all experiments was purified, obtained from Millipore.

Preparation of BHR-SLNs

BHR-SLNs were prepared using the emulsification–evaporation technique. Briefly, BHR (10 mg), stearic acid (0.1 g), and acetone were dissolved in 10 mL chloroform in a glass flask. The organic phase was then prepared by dissolving 0.1 g lecithin in 5 mL chloroform and moving the resulting solution to the flask containing the BHR. To make the aqueous phase, 0.3 g Myrj 59 was dissolved in 30 mL water and the subsequent solution was heated to 75±2°C in a water bath.

Next, the organic phase was added to the aqueous phase while stirring at 1,000 rpm at 75°C. The stirring continued for approximately 4 h, allowing enough time for the organic solvent to completely evaporate and the volume of the mixture to condense to approximately 5 mL. The flask was then removed from the water bath, 10 mL of ice-cold (0–2°C) water was added, and the mixture was stirred again at 1,000 rpm for 2 h. The resulting suspension was centrifuged in a superspeed refrigerated centrifuge (Avanti J-25, Beckman Coulter) at 20,000 rpm and 4°C for 2 h to isolate and subsequently remove the supernatant. The pellet was resuspended in ultrapure water, placed in −80°C for 1 h, and lyophilized in a tabletop lyophilizer.

Lyophilization was carried out in a lyophilizer (FDU-1100/DRC-1000, Eyela Inc., Japan) as follows: (1) the samples were cooled from 25°C to −45°C at a rate of 0.5°C/min and then maintained at −45°C for 4 h; (2) primary drying was carried out at −37°C, −30°C, and −16°C for 2 h, respectively; and secondary drying was carried out at 25°C for 4 h. The chamber pressure was maintained below 3 Pa during the drying process. When the freeze-drying process was complete, the vials containing the lyophilized powders were filled with nitrogen gas, sealed, and stored at 4°C. During the lyophilization process, a certain amount of trehalose was added as a stabilizing agent.

Photon Correlation Spectroscopy and Zeta Potential Measurement of BHR-SLNs

Photon correlation spectroscopy (PCS; LS230 Beckman Coulter) at 25°C under a fixed angle of 90° in disposable polystyrene cuvettes was used to measure the average particle size (*z*-average size) and size distribution of our BHR-SLNs. The measurements were recorded using a red helium neon (633 nm) laser. The zeta potential was measured by laser Doppler velocimetry (Zetasizer 3000, Malvern Instruments, Malvern, UK) at 25°C.

Transmission Electron Microscopy and Atomic Force Microscopy of BHR-SLNs

The surface morphology of the BHR-SLNs was evaluated using a JEM-1230 TEM (JEOL). A carbon-coated 200-mesh copper specimen grid was glow-discharged for 1.5 min. A drop of diluted suspension of BHR-SLNs was deposited on the grid and left alone for 1.5 min. Excess fluid was removed using filter paper. The grid was then stained with one drop of 2% phosphotungstic acid and air-dried for 10 min before examination via transmission electron microscopy (TEM).

The surface morphology of prepared BHR-SLNs was also visualized by atomic force microscopy (AFM; SPA 3800N, SEIKO, Japan). Explorer AFM was in tapping mode, using high resonant frequency (F_0=129 kHz) pyramidal cantilevers with silicon probes having force constants of 20 N/m. Scan speeds were set at 2 Hz. The samples were diluted 10 times with water and then dropped onto freshly cleaved mica plates, followed by vacuum drying at 25°C for 24 h.

Stability Studies of BHR-SLN

The chemical and physical stabilities of BHR-SLN were evaluated via clarity, particle size, and zeta potential. The synthesized BHR-SLNs were portioned and some were used to test their stability: five portions were stored at room temperature and another five portions were stored at 4°C. After 24 h, 1 month, 3 months, and 6 months, the stability of the BHR-SLNs was assessed. The centrifuge test was also carried out to assess the physical stability of the BHR-SLN. The BHR-SLNs were then centrifuged at 5,000 rpm for 30 min in the centrifugation test.

Fourier Transform Infrared Spectra of BHR-SLNs

Fourier transform infrared (FT-IR) spectra were obtained on a Bruker Vector 22 spectrophotometer by the conventional KBr pellet method (sample/KBr=1/100). The samples were ground gently with anhydrous KBr and compressed to form pellets. The scanning range was 4,000–500 cm^{-1} and the resolution was 4 cm^{-1}.

Entrapment Efficiency of BHR-SLNs

BHR was analyzed by HPLC (Agilent 1100 series, Agilent, USA) using a C18 column (25 cm×4.6 mm, 5 μm). For the mobile phase, a methanol–water mixture (60: 40, *v*/*v*) and flow rate of 1 ml/min was used. The detection wavelength was set at 300 nm and the retention time was about 6 min. The controlled solution (10–75 μg/mL) was prepared by dissolving BHR (precisely weighed) in the mobile phase. Drug recovery was calculated as follows:

$$Drug\ recovery = \frac{analyzed\ weight\ of\ BHR\ in\ SLNs}{theroetical\ weight\ of\ BHR\ loaded\ in\ system} \times 100\%$$

The BHR-SLN suspension was separated by gel filtration chromatography using a Sephadex G50 column. After diluting with methanol, the concentrations of free BHR (n_2) and BHR

in the suspension (n_1) were measured by HPLC. EE% was then calculated as follows:

$$EE(\%) = \frac{n_1 - n_2}{n_1} \times 100\%$$

In Vitro Release Study

The drug release from SLNs was assessed by dialyzing against 50 mL of phosphate buffer (pH 7.4 and pH 4.8) in a beaker. The buffers were stirred at 150 rpm at 37°C and replaced with 50 mL of fresh solution at predetermined time intervals (2, 4, 6, 8, 12, 16, 20, 24, 28, 32, 36, and 48 h). The solutions removed at each time point were analyzed via HPLC to measure the amount of BHR released from the SLNs. These measurements were utilized to illustrate the *in vitro* release profile of BHR-SLNs, as well as the relationship between the release rate and time. This drug release study was done in triplicate.

Cellular Cytotoxicity Assays of BHR-SLN

The cytotoxicity of BHR, SLNs, and BHR-SLNs to 293T and Hela cells was measured using the MTT assay. Cell lines were routinely cultured in RPMI-1640 with 10% FCS and incubated at 37°C in a humidified incubator supplied with 5% CO_2. To test cytotoxicity, cells were plated in a 96-well plate at a density of about 2×10^4 cells per well and subsequently incubated at 37°C in a humidified incubator supplied with 5% CO_2 for 24 h. Different concentrations of BHR, BHR-SLNs (10, 20, 30, and 40 μg/mL), or PBS (negative control) were added to the cells (three wells per group) and incubation was continued under the same previously stated conditions for another 48 h. MTT dye solution (20 μL; 5 mg/mL) was added to each well and allowed to incubate for 4 h at 37°C. The MTT solution was then removed, cells were subsequently treated with 150 μL DMSO, and the absorbance at 590 nm was measured using a microplate reader (ELX 800 UV, BIO-TEK, USA). Cell viability was calculated as follows:

$$Cell\ viability(\%) = \frac{OD_{590(sample)} - OD_{590(blank)}}{OD_{590(control)} - OD_{590(blank)}} \times 100\%$$

Statistical Analysis

For statistical analysis, the data gathered from the *in vitro* release and cytotoxicity studies were presented as the mean± standard deviation of three independent experiments. Groups were first compared via one-way analysis of variance followed

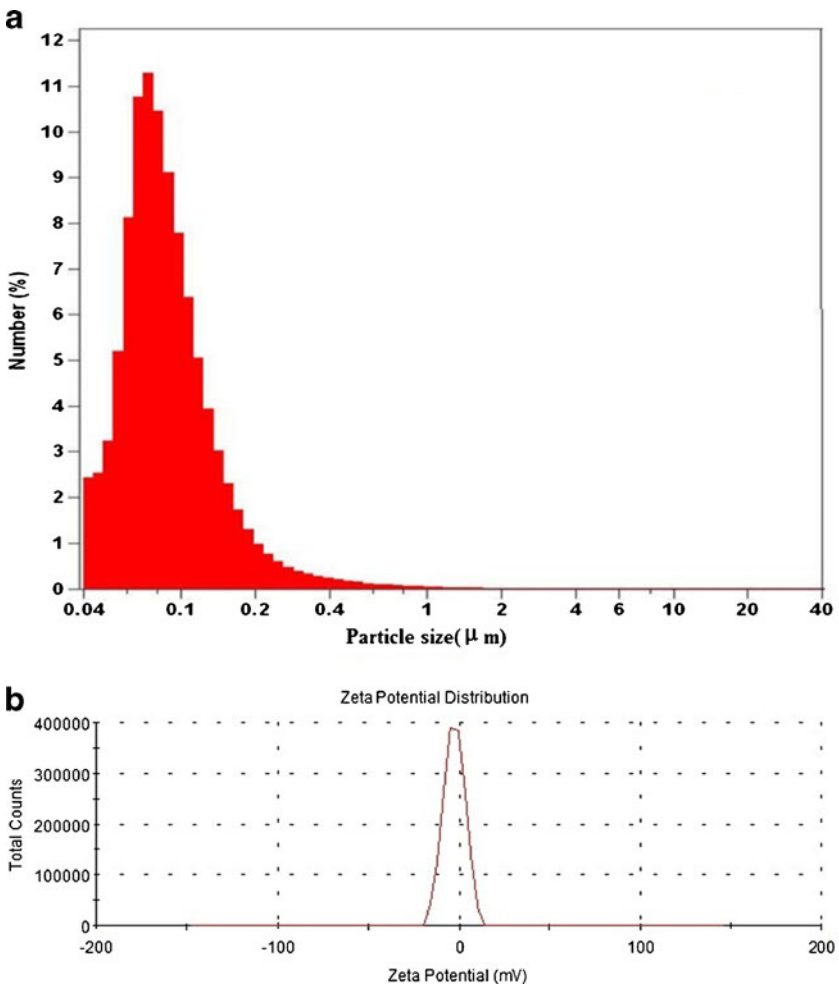

Fig. 2. **a** Particle size distribution and **b** zeta potential distribution of BHR-SLNs

by *t* tests for pairwise comparisons. The SPSS program was used to perform these statistical analyses and determine the levels of significance for each result.

RESULTS AND DISCUSSION

Particle Size and Zeta Potential Measurement of BHR-SLNs

PCS was used to measure the particle size and size distribution of BHR-SLNs (Fig. 2a). On average, the BHR-SLNs were about 75 nm, with the diameters of 91.9% of the particles between 45 and 200 nm. We did not observe any multiscattering phenomenon. Additionally, the zeta potential of the nanoparticles was −2.66 mV (Fig. 2b).

TEM and AFM Examinations of BHR-SLN Nanoparticles

As observed via TEM, BHR-SLNs were spherical in shape (Fig. 3). The electron micrographs also confirmed the diameters and size distribution that was observed via PCS (Fig. 2).

AFM was adapted to study the dehydrated state of SLNs, since such sample preparation did not require pretreatment and the results more closely resembled those obtained by PCS than by scanning electron microscopy (26). The AFM images of BHR-SLNs showed spherical particles that were accumulated to a great extent (Fig. 4). They also indicated that the BHR-SLNs were about 200 nm long and wide and about 40 nm in height. The length of the BHR-SLNs observed via AFM was five times the height, which might be due to the accumulation of nanoparticles.

Stability Studies of BHR-SLN Nanoparticles

The samples kept at 4°C and at room temperature remained homogenous after 1 month. No obvious precipitation or crystallization occurred, indicating that this system was stable. A little precipitation of the samples at room temperature occurred after 3 months. The samples kept at 4°C did not precipitate by the 3-month time point, but did after 6 months. However, the precipitation disappeared almost immediately after being shaken. The particle size of BHR-SLN stored for 6 months is 73.28 nm, which did not show obvious changes over the observation period. The centrifuge test also showed that the BHR-SLN had a good physical stability. Table I shows the particle size, polydispersity index (PDI), and zeta potential of the SLN and BHR-SLN after storage for 3 and 6 months.

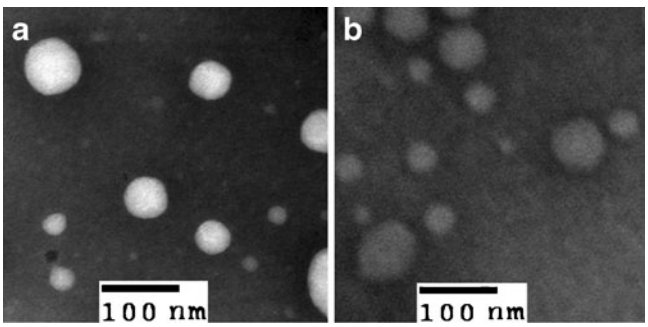

Fig. 3. Images of SLNs (**a**) and BHR-SLNs (**b**) obtained by TEM after being stained with one drop of 2% phosphotungstic acid

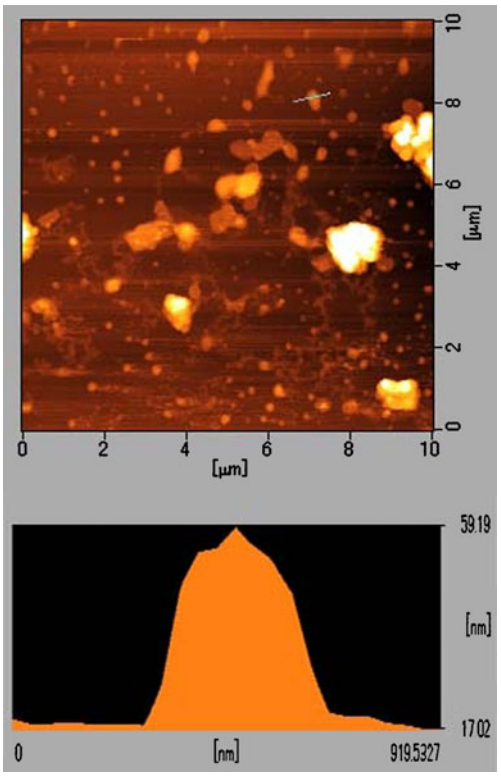

Fig. 4. AFM images of BHR-SLNs utilized for the analysis of particle size

The physicochemical properties of nanoparticles are associated with their physical stability, cellular uptake, and biodistribution *in vivo*. An average particle size below 100 nm is considered optimum for administration by injection. This size also facilitates the uptake of nanomaterials by cells (8). In this study, the average size of our BHR-SLNs was 75 nm. Therefore, BHR-SLNs are suitable for application in cell and animal experiments. The negative charge of the particles makes the particles repel each other, thereby keeping the BHR-SLNs stable.

FT-IR Analysis of BHR-SLNs

FT-IR spectroscopy was used to detect the conformations of lipid molecules in matrices. Figure 5 shows the BHR, SLN, and BHR-SLNs FT-IR spectra from 500 to 4,000 cm^{-1}. The broad absorption band at approximately 3,400–3,200 cm^{-1} was due to stretching of the –OH groups in BHR and BHR-SLNs nanoparticles. The strong peak range around 2,900 cm^{-1} was from the stretching vibration of $–CH_2$. The strong absorption

Table I. The Particle Size, PDI, and Zeta Potential of the SLN and BHR-SLN After Storage for 3 and 6 Months

Samples	Particle size (nm)	Zeta potential	PDI
SLN (3 months)	72.88	−5.35	0.339±0.003
SLN (6 months)	70.49	−4.80	0.342±0.007
BHR-SLN (3 months)	74.32	−2.59	0.287±0.006
BHR-SLN (6 months)	73.28	−2.02	0.291±0.005

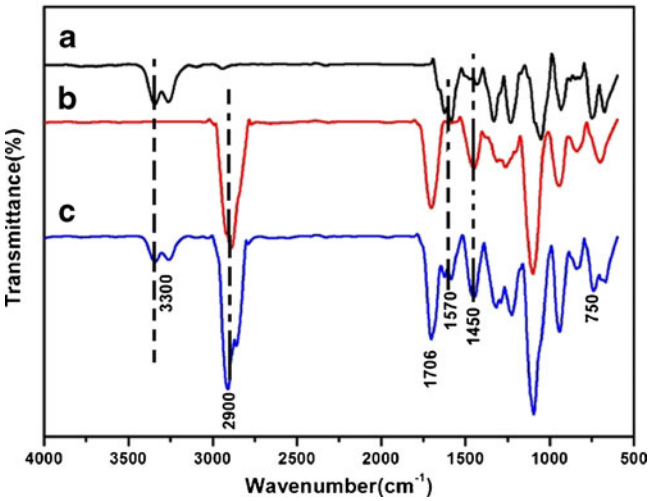

Fig. 5. FT-IR spectra of *a* BHR, *b* SLN, *c* BHR-SLNs

bands at 1,706 cm^{-1} indicated the presence of the C=O group in lipids (27). In addition, the absorption bands at 1,570 cm^{-1} represented the stretching vibrations of C=C in the backbone of the aromatic ring, which can only be seen in BHR and BHR-SLN samples. The absorption band at 1,450 cm^{-1} was due to the stretching vibrations of C–O of stearic acid in SLN and BHR-SLIN (28). These results indicated that BHR was successfully encapsulated in SLNs.

Entrapment Efficiency of BHR-SLNs

The amount of drug incorporated into a delivery vehicle depends on the physicochemical properties of the drug and the preparation process. A sufficient loading capacity may only be achieved if the drug is highly soluble in melted lipid. Fortunately, one of the major advantages of SLNs is their comparatively high drug EE%.

The recovery from preparation ranged from 99.09% to 100.92%, with the mean value being 99.97%. Approximately

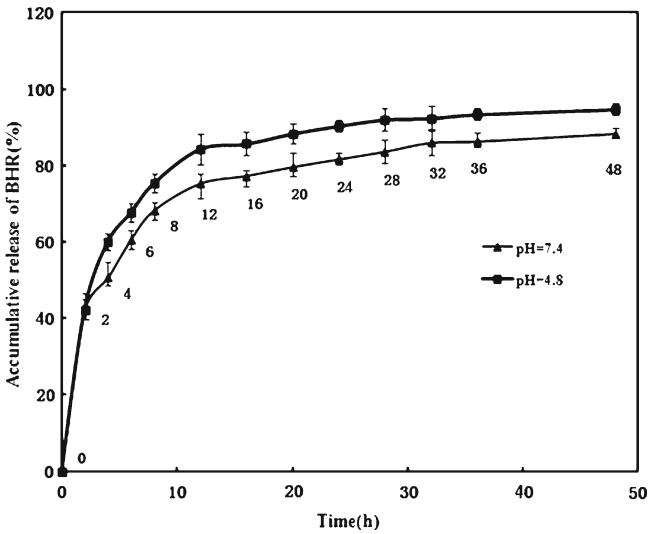

Fig. 6. Accumulative release profile of BHR from SLNs into phosphate buffer (pH 7.4 and pH 4.8) for 48 h. BHR were released from the SLNs in a slow but gradual time-dependent manner with an initial burst release within the first 2 h

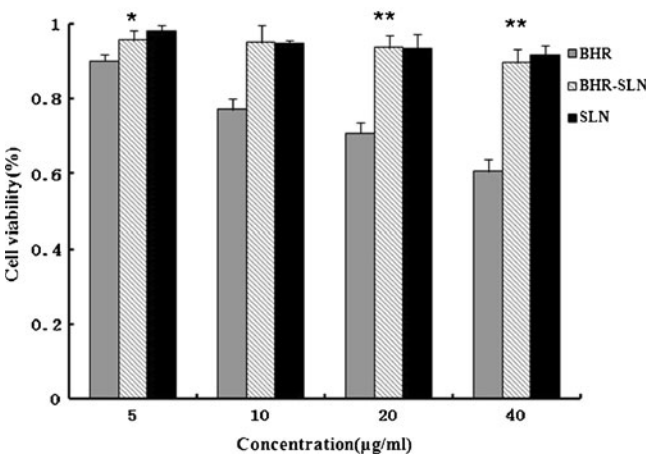

Fig. 7. Cytotoxicity of SLNs, BHR, and BHR-SLNs of different BHR concentrations to 293T cells after 48 h exposure. Results represent the means of three independent experiments, and *error bars* represent the standard error of the mean. $N=3$, $*p<0.05$; $**p<0.001$

70.2% of BHR used was incorporated inside and on the surface of the SLNs. This high EE% implies that SLNs are appropriate delivery vehicles for BHR.

In Vitro Release of BHR-SLNs

As depicted in the *in vitro* drug release profile of BHR-SLNs (Fig. 6), drug release in the pH 7.4 and pH 4.8 buffers was able to last for 48 h. There were initial burst releases in the first 2 h. The underlined mechanism of this phenomenon might perhaps be due to the skeleton structure of the BHR-SLNs. Such a structure contains a large surface area to which some of the drug was adsorbed, while the rest could be found inside the skeleton structure. As a result, the initial burst release could be from the adsorbed drug being quickly released from the surface. The remaining drug would then be released from the skeleton structure, accounting for the continuous gradual release seen in the later phase. Even after 48 h, the drug was still being released

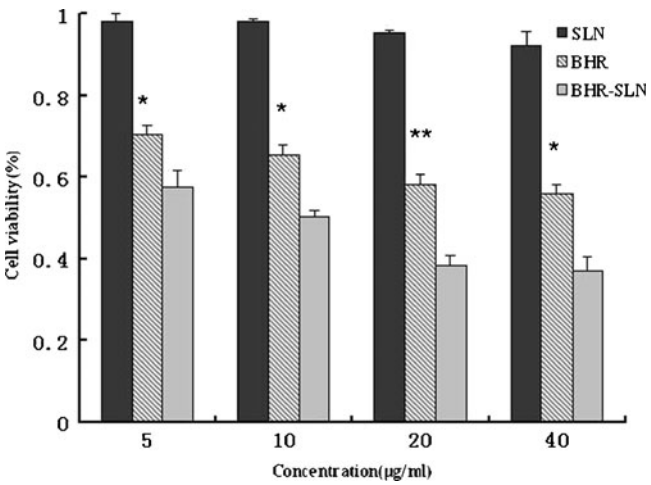

Fig. 8. Survival ratio of Hela cells treated with SLNs, BHR, and BHR-SLNs with different BHR concentrations after 48 h exposure. Results represent the means of three independent experiments, and *error bars* represent the standard error of the mean. $N=3$, $*p<0.05$; $**p<0.001$

at a relatively constant rate from the SLNs, indicating that the BHR was stably bound in the SLNs.

Hydrogen ions tend to accumulate in rapidly growing tumor tissue, mainly due to their high metabolic rates and inadequate waste transport systems. This may result in severe tissue acidosis, especially in bulky and/or low-flow tumors (29). Ideal anticancer drug delivery systems should be able to specifically target and kill cancer cells while sparing normal cells. To exploit the pH difference between normal and cancerous tissue, various investigations on fabricating pH-sensitive drug delivery systems have been reported (30,31). Since cancerous tissues usually contain more acidic microenvironments, delivery systems having distinct release profiles in different pH levels would be an invaluable approach for anticancer chemotherapy (32). In our study, a higher release rate of BHR was achieved at lower pH (Fig. 6). Therefore, the entrapped BHR in the SLNs has a greater tendency to be released into a more acidic environment, which, to some degree, may be helpful for the release of BHR in acidic cancerous tissues. The favored release would result in a higher release rate of BHR in tumor tissues, which indicates that BHR-SLNs would likely exhibit specificity of BHR release in cancerous tissue and inhibit the proliferation of cancer cells.

Cellular Cytotoxicity Assays of BHR-SLNs

The cytotoxicity of SLNs, BHR-SLNs, and BHR was evaluated via bioassay using 293T and Hela cells. As shown in Fig. 7, SLNs do not have any significant effect on the proliferation of 293T normal cells; the cytotoxicity of BHR and BHR-SLNs against 293T cells was enhanced with increasing density of BHR. Especially after the drug was encapsulated in SLNs, BHR-SLNs showed no obvious cytotoxicity with increasing dose of BHR. BHR-SLNs were less toxic to 293T cells compared with BHR of the same concentration. Moreover, the difference between BHR and BHR-SLNs was significant in all concentrations. Thus, SLNs, as carriers of BHR, can effectively reduce the cytotoxicity of BHR to normal cells.

BHR and BHR-SLNs suppressed the proliferation of tumor cells, whereas SLNs alone exerted no significant effect (Fig. 8). Moreover, BHR-SLNs had higher tumor suppression efficiency compared to BHR of the same concentration. These results indicate that BHR-SLNs are more efficient for cancer treatment than BHR alone; the cell viability of tumor cells treated with BHR-SLNs was much lower than the viability of those treated with BHR alone after 2 days. It seemed that the BHR molecules were stabilized when they were entrapped in SLNs. Moreover, it can be inferred that BHR-SLNs could be more easily taken up by Hela cells and their sustained release profile could imply prolonged exposure time. It also seemed that BHR-SLNs preferred tumor cells to normal cells. The possible reason might be due to the different pH values between tumor cells and normal cells; BHR-SLNs have the pH-sensitive tendency to low pH in relatively acidic extracellular fluids in the tumor or after endocytosis in the endosomes or lysosomes in tumor cells (33). These would allow more tumor cells to be affected by BHR and thereby increase drug efficiency (6,14).

CONCLUSIONS

BHR-SLNs were successfully prepared using the emulsification–evaporation technique. The average particle size was approximately 75 nm and the EE% was approximately 70.2%. Our *in vitro* release study demonstrated that BHR-SLNs exhibit a slow-release profile, which directly leads to enhanced drug efficiency. The cytotoxicity assay demonstrated that the cytotoxicity of BHR to normal cells was effectively weakened and the inhibitive effect of BHR on tumor cells was enhanced by using SLNs as carriers. Therefore, SLNs can be considered ideal carriers for BHR. In addition, BHR-SLNs are a potential anticancer drug delivery system with a range of new therapeutic applications.

ACKNOWLEDGMENTS

This work was supported by the 973 Project of the Ministry of Science and Technology (nos. 2010CB912604 and 2010CB933901), the National Natural Science Foundation of China (no. 31100855), the Program for Young Excellent Talents in Tongji University(no. 2000219054), The Genetically Modified Organisms Breeding Major Projects (no. 2009ZX08011-032B), and the Shanghai Key Laboratory of Cell Signaling and Diseases (grant no. 09DZ2260100).

REFERENCES

1. Owen RW, Giacosa A, Hull WE, Haubnerelhalder B, Bartsch H. The antioxidant/anticancer potential of phenolic compounds isolated from olive oil. Eur J Cancer. 2000;36:1235–47.
2. Guilherme AS, Cristiane MF, Mauro SP, Patricia Z. Acetylsalicylic acid and salicylic acid decrease tumor cell viability and glucose metabolism modulating 6-phosphofructo-1-kinase structure and activity. Biochem Pharmacol. 2009;77:46–53.
3. Bayram E, Senturk M, Kufrevioglu OI, Supuran CT. *In vitro* inhibition of salicylic acid derivatives on human cytosolic carbonic anhydrase isozymes I and II. Bioorg Med Chem. 2008;16:9101–5.
4. Salzmann U, Ludwig P, Schewe I, Rapoport SM. The share of lipoxygenase in the antimycin-resistant oxygen uptake of rabbit reticulocytes. Biomed Biochim Acta. 1985;44:213–21.
5. Wang M, Cheng LL, Zhu H, Li K, Wu QS, Yao SD, *et al*. Characterization of the transient species generated in the photoexcitation of benzoic acid, 2-hydroxy, 2-D-ribofuranosylhydrazide. J Photochem Photobiol. 2009;208:104–9.
6. Zhu RR, Qin LL, Wang M, Wu SM, Wang SL, Zhang R, *et al*. Preparation, characterization and anti-tumor property of podophyllotoxin-loaded solid lipid nanoparticles. Nanotechnology. 2009;20:055702. doi:10.1088/0957-4484/20/5/055702.
7. Qin LL, Wang SL, Zhang R, Zhu RR, Sun XY, Yao SD. Two different approaches to synthesizing Mg-Al-layered double hydroxides as folic acid carriers. J Phys Chem Solids. 2008;69:2779–84.
8. Qin LL, Xue M, Wang WR, Zhu RR, Wang SL, Sun J, *et al*. The *in vitro* and *in vivo* anti-tumor effect of layered double hydroxides nanoparticles as delivery for podophyllotoxin. Int J Pharm. 2010;388:223–30.
9. Li A, Qin LL, Zhu D, Zhu RR, Sun J, Wang SL. Signaling pathways involved in the activation of dendritic cells by layered double hydroxide nanoparticles. Biomaterials. 2010;31:748–56.
10. Li A, Qin LL, Wang WR, Zhu RR, Yu YC, Liu H, Wang SL. The use of layered double hydroxides as DNA vaccine delivery vector for enhancement of anti-melanoma immune response. Biomaterials. 2011;32:469–77.
11. Xue YH, Zhang R, Sun XY, Wang SL. The construction and characterization of layered double hydroxides as delivery vehicles for podophyllotoxins. Mater Sci Mater Med. 2007;8:1197–202.

12. Xu ZP, Zeng QH, Lu GQ, Yu AB. Inorganic nanoparticles as carriers for efficient cellular delivery. Chem Eng Sci. 2006;61:1027–40.
13. Wang WR, Zhu RR, Xiao R, Liu H, Wang SL. The electrostatic interactions between nano-TiO_2 and trypsin inhibit the enzyme activity and change the secondary structure of trypsin. Biol Trace Elem Res. 2010;142:435–46.
14. Muller RH, Mader K, Gohla S. Solid lipid nanoparticles (SLN) for controlled drug delivery—a review of the state of the art. Eur J Pharm Biopharm. 2000;50:161–77.
15. Mehnert W, Mader K. Solid lipid nanoparticles: production, characterization and applications. Adv Drug Deliv Rev. 2001;47:165–96.
16. Wissing SA, Muller RH. Cosmetic applications for solid lipid nanoparticles (SLN). Int J Pharm. 2003;254:65–8.
17. Li YC, Dong L, Jia A, Chang XN, Xue H. Preparation and characterization of solid lipid nanoparticles loaded traditional Chinese medicine. Int J Biol Macromol. 2006;38:296–9.
18. Uner M. Preparation, characterization and physico-chemical properties of solid lipid nanoparticles (SLN) and nanostructured lipid carriers (NLC): their benefits as colloidal drug carrier systems. Pharmazie. 2006;61:375–86.
19. Muller RH, Radtke M, Wissing SA. Solid lipid nanoparticles (SLN) and nanostructured lipid carriers (NLC) in cosmetic and dermatological preparations. Adv Drug Deliv Rev. 2002;54:131–55.
20. Liu J, Gong T, Wang C, Zhong Z. Solid lipid nanoparticles loaded with insulin by sodium cholate-phosphatidylcholine-based mixed micelles: preparation and characterization. Int J Pharm. 2007;340:153–62.
21. Suresh G, Manjunath K, Venkateswarlu V, Satyanarayana V. Preparation, characterization, and *in vitro* and *in vivo* evaluation of lovastatin solid lipid nanoparticles. AAPS Pharm Sci Tech. 2007;8:162–70.
22. Blasi P, Giovagnoli S, Schoubben A, Ricci M, Rossi C. Solid lipid nanoparticles for targeted brain drug delivery. Adv Drug Deliv Rev. 2007;59:454–77.
23. Chen HB, Chang XL, Du DR, Liu W. Podophyllotoxin-loaded solid lipid nanoparticles for epidermal targeting. J Control Release. 2006;110:296–306.
24. Kim JH, Kim YS, Park K, Kang E, Lee S, Nam HY, *et al*. Self-assembled glycol chitosan nanoparticles for the sustained and prolonged delivery of antiangiogenic small peptide drugs in cancer therapy. Biomaterials. 2008;29:1920–30.
25. You J, Wan F, Cui FD, Sun Y, Du YZ, Hu FQ. Preparation and characteristic of vinorelbine bitartrate-loaded solid lipid nanoparticles. Int J Pharm. 2007;343:270–6.
26. Dubesa A, Parrot-Lopeza H, Abdelwahed W. Scanning electron microscopy and atomic force microscopy imaging of solid lipid nanoparticles derived from amphiphilic cyclodextrins. Eur J Pharm Biopharm. 2003;55:279–82.
27. Garg A, Singh S. Enhancement in antifungal activity of eugenol in immunosuppressed rats through lipid nanocarriers. Colloids Surf B Biointerfaces. 2011;87:280–8.
28. Lin XL, Li XW, Zheng Yu L, Zhang QQ, Liu WC. Preparation and characterization of monocaprate nanostructured lipid carriers. Colloids Surf, A Physicochem Eng Asp. 2007;311:106–11.
29. Vaupel P, Kallinowski F, Okunieff P. Blood flow, oxygen and nutrient supply, and metabolic microenvironment of human tumors: a review. Cancer Res. 1989;49:6449–65.
30. Kang SI, Na K, Bae YH. Physicochemical characteristics and doxorubicin release behaviors of pH/temperature-sensitive polymeric nanoparticles. Colloids Surf, A Physicochem Eng Asp. 2003;231:103–12.
31. Liu L, Jin P, Cheng M, Zhang G, Zhang F. 5-Fluorouracil-loaded self-assembled pH-sensitive nanoparticles as novel drug carrier for treatment of malignant tumors. Chin J Chem Eng. 2006;14:377–82.
32. Robhash KS, Keon WK, Hoo-Kyun C. Preparation and characterization of solid lipid nanoparticles loaded with doxorubicin. Eur J Pharm Sci. 2009;37:508–13.
33. Martins S, Costa-Lima S, Carneiro T, Cordeiro-da-Silva A, Souto EB, Ferreira DC. Solid lipid nanoparticles as intracellular drug transporters: an investigation of the uptake mechanism and pathway. Int J Pharm. 2012;430:216–27.